Acta Biochim Biophys Sin 2024, 56(2): 304–314
https://doi.org/10.3724/abbs.2024006
Advance Access Publication Date: 26 January 2024
Original Article

Original Article

ATIP/ATIP1 regulates prostate cancer metastasis through mitochondrial dynamic-dependent signaling

Haokun Yuan[1,2,†], Ruiqin Fang[3,†], Chi Fu[2], Shuo Wang[2], Xiaoqin Tong[2], Deyi Feng[4], Xiaoqing Wei[2], Xirong Hu[2], and Yuan Wang[1,2,*]

[1]The Key Laboratory for Human Disease Gene Study of Sichuan Province and the Department of Laboratory Medicine, Sichuan Provincial People's Hospital, School of Medicine, University of Electronic Science and Technology of China, Chengdu 610072, China, [2]The School of Medicine, University of Electronic Science and Technology of China, Chengdu 610054, China, [3]The School of Life Science, University of Electronic Science and Technology of China, Chengdu 610054, China, and [4]State Key Laboratory of Cellular Stress Biology, School of Life Sciences, Xiamen University, Xiamen 361104, China

[†]These authors contributed equally to this work.

*Correspondence address. Tel: +86-28-83201072; E-mail: wangyuan_med@uestc.edu.cn

Received 21 August 2023 Accepted 24 December 2023

Abstract

Mitochondria play a fundamental role in cell survival and motility. Abnormalities in mitochondria are associated with carcinogenesis, especially with tumor metastasis. In this study, we explore the biological function of ATIP1, which is a mitochondrial-located isoform of angiotensin II AT2 receptor interacting proteins (ATIPs) in prostate cancer cells. The results showed that ATIP is downregulated in prostate cancer tissues and is negatively correlated with the disease-free survival rate of prostate cancer patients. Silencing of *ATIP* promotes mitochondrial fission and enhances tumor cell migration and invasion. Reconstitution of ATIP1 in ATIP-deficient cells significantly attenuates mitochondrial trafficking and tumor cell movement. Therefore, ATIP1 is a negative regulator of mitochondrial dynamics and tumor cell motility and is also a potential biomarker for predicting prostate cancer malignancy.

Key words ATIP/ATIP1, Drp1, mitochondrial dynamics, metastasis

Introduction

A hallmark of cancer is tissue invasion and metastasis [1]. Mitochondria exist as a dynamic network and are critical for multiple cellular functions, including cell growth, cell death and cell metastasis [2–5]. Morphologically, mitochondria are characterized by highly dynamic structures of long interconnected tubules with short isolated dots, which are controlled by a series of large GTPase proteins through interchange of fission and fusion events [6]. Mitochondrial fusion is controlled by Mitofusin 1/2 (Mfn1/2) [7] and optic atrophy 1 (OPA1) [8], and fission is modulated by dynamin-related protein 1 (Drp1) [9], fission protein 1 (Fis1) [10] and mitochondrial fission factor (Mff) [11]. Dysfunction of these large GTPase proteins could result in abnormalities in mitochondrial shape/size and subcellular position, which in turn can lead to an incomplete energy supply in response to stimulation from the extracellular environment [6,12].

Accumulating evidence suggests that an imbalance in mitochondrial fission and fusion is strongly associated with tumorigenesis [13], including metabolic reprogramming [14], immune escape [15] and biogenesis[16]. Compared with normal tissues, mitochondrial fragmentation occurs more frequently in multiple cancer cell types, including breast cancer [17], pancreatic cancer [18], melanoma [19] and neuroblastoma [20]. In addition, various mitochondrial proteins are involved in the regulation of tumor cell movement through the activation of mitochondrial fission. For instance, wild-type mitochondrial isocitrate dehydrogenase 2 (IDH2) promotes prostate cancer metastasis by excessively activating mitochondrial division, whereas inhibition of the mitochondrial fission process can rescue the invasion associated with *IDH2* knockdown [21]. Disrupting the ubiquitination of the mitochondrial protein SNPH increases the recruitment of Drp1 to mitochondria and promotes tumor cell motility [22].

The angiotensin II AT2 receptor interacting protein (ATIP), also known as microtubule-associated tumor suppressor 1 gene (MTUS1), is located in the 8p22 chromosomal region. The *ATIP* gene encodes 4 protein isoforms, ATIP1, ATIP2, ATIP3 and ATIP4

[23,24]. ATIP1 and ATIP3 are the two major splice variants. The ATIP1 and ATIP3 transcripts exhibit ubiquitous profiles with different expression levels, varied subcellular localizations and diverse biofunctions.

ATIP3 localizes to the microtubule cytoskeleton and the centrosome in interphase, whereas it is shuttled to the mitotic spindle during mitosis. Therefore, ATIP3 is associated with the stability of microtubules [25] and is involved in the regulation of the cell cortex and subsequent cell polarity and migration [26]. ATIP3 depletion promotes breast cancer cell migration, front-rear polarity and microtubule dynamics [27,28], but paradoxically sensitizes breast cancer cells to chemotherapy [29]. ATIP1 localizes to mitochondria and is also regarded as a tumor suppressor. Ranjan *et al.* [30] found that ATIP1 expression was downregulated in malignant glioma, probably due to promoter hypermethylation. Furthermore, high ATIP1 expression might retard the response to radiation therapy by enhancing double-strand DNA break repair [30]. ATIP1 participates in p53-involved tumor signal transduction through binding between the *ATIP1* promoter and p53 [31].

Recent studies have shown that ATIP expression is closely associated with poor prognosis in patients with various cancers, including lung adenocarcinoma [32], breast cancer [25], colorectal cancer [33], bladder cancer [34], salivary adenoid cystic carcinoma [35] and renal cell carcinoma [36]. Prostate cancer, the third leading cause of cancer death in middle-aged men worldwide, is among the most common urological malignancies, and malignancy of prostate cancer has been found to be associated with ATIP expression [37]. Compared with that in the more metastatic prostate cancer cell line PC3, ATIP1 expression is higher in the less metastatic prostate cancer cell line LNCaP [38]. Interestingly, there is no observable difference in ATIP3 expression between these two cell lines [38,39]. Unfortunately, the detailed regulatory mechanism of ATIP is largely unknown.

In our study, we found that ATIP expression is downregulated in prostate cancer patients, which negatively correlates with cell migration, invasion and mitochondrial dynamics. ATIP1, a major isoform of ATIP family, has been identified as a key regulator of mitochondrial-directed prostate cancer cell motility. The re-expression of ATIP1 in ATIP-deficient cells retards the mitochondrial fission process and downregulates focal adhesion kinase, ultimately inhibiting 2D motility. Moreover, specific *ATIP1* silencing in PC3 cells significantly promotes distant metastasis *in vivo*. Taken together, these findings indicate that ATIP/ATIP1 plays a potential role in regulating tumor metastasis and in predicting tumor prognosis.

Materials and Methods

Analysis of GEO datasets

Prostate cancer gene expression profiles and clinical data were downloaded from the GSE21034 dataset. The statistical analyses were performed using R software (v4.0.0). When observing the expression of the ATIP gene in patients with different Gleason grades, we excluded patients with grade 5 because only one patient was included. We defined patients who experienced recurrence as 'recurrence' and patients who did not experience recurrence or who had been followed up for more than 3 years as 'non-recurrence'. The Wilcoxon test was used for pairwise comparisons. Kaplan–Meier and log-rank tests were used for survival analysis. The optimal cutoff value of ATIP expression was determined by the "surv_cutpoint" function of survminer R package (v0.4.9).

Cells and cell culture

Cell culture experiments were carried out in multiple model systems. Prostate adenocarcinoma PC3 cells were obtained from Procell Life Science & Technology (Wuhan, China) and cultured according to the supplier's specifications. Conditioned medium used for cell invasion/migration assays was collected from NIH3T3 cells which were cultured in Dulbecco's modified Eagle's medium (Shanghai Yuanpei Biotechnology Co., Ltd., Shanghai, China) supplemented with sodium pyruvate, 10 mM HEPES, and 10% fetal bovine serum for 2 days.

Antibodies and reagents

Antibodies against focal adhesion kinase (FAK), phosphorylated FAK (Tyr925), Drp1, Ser616-phosphorylated Drp1, MFN1 and MFN2 were purchased from Cell Signaling Technology (Danvers, USA). The anti-ATIP antibody was purchased from GeneTex (Irvine, USA). MitoTracker Deep Red was purchased from Thermo Fisher Scientific (Waltham, USA), and the antibody against actin was obtained from Santa Cruz Biotechnology (Dallas, USA).

Plasmid construction

cDNA sequences for ATIP1 and ATIP3, which were fused with a Flag tag at the C-terminus, were inserted into the pCMV5 vector. siRNA-resistant mutants were generated by introducing silent mutations at the siRNA target sites. The above mutants were generated with a QuikChange site-directed mutagenesis kit (Stratagene, La Jolla, USA) and verified by sequencing.

Small interfering RNA (siRNA) transfection

Gene knockdown experiments with small interfering RNA (siRNA) were carried out as previously described by Wang *et al.* [21]. The siRNA for negative control (NTC), ATIP siRNA and Drp1 siRNA were purchased from RiboBio Company (Guangzhou, China). The sequences are listed as follows: NTC siRNA: 5′-GCGCGCTTTGTAGGATTCG-3′; ATIP siRNA #1: 5′-GCTTCGGGACACTTACATT-3′; ATIP siRNA #2: 5′-GCAATTGCAAGAGCAGTTT-3′; and Drp1 siRNA: 5′-GGAGTAAGCCCTGAACCAA-3′.

PC3 cells were transfected with various siRNAs at a concentration of 40 nM using Lipofectamine RNAiMax (Thermo Fisher Scientific) at a 1:1 ratio (volume of siRNA 20 mM to volume of Lipofectamine RNAiMax). After 72 h, the knockdown efficiency of the target protein was validated by western blot analysis in transfected cells, after which the proteins were subjected to functional experiments. ATIP1 and ATIP3 cDNA were introduced into PC3 cells using Lipofectamine 2000 (Thermo Fisher Scientific) following the manufacturer's instructions.

Real-time PCR

Total RNA was extracted from PC3 cells using TRIzol (Invitrogen, Carlsbad, USA) according to the manufacturer's protocol. One microgram of total RNA from each sample was reverse transcribed with SuperScript® II Reverse Transcriptase (Thermo Fisher Scientific). The resulting complementary DNA (cDNA) was analyzed by real-time PCR using SYBR Green dye. All gene expression results were expressed as arbitrary units relative to the expression of *GAPDH*. Real-time PCR primers used for the ATIPs are listed in Table 1.

Table 1. The sequence of primers used for real-time PCR

ATIP isoform	Forward primer (5′→3′)	Reverse primer (5′→3′)
ATIP1	TGTGAAATCTCGCCACCTGC	GAGCTGTCTGTGGCTGGATA
ATIP2	AAGTAGCTGCATACCCTGGC	TGATGACAGCGGCATTACCA
ATIP3	CCACAGTGAGCTGAGCACTT	AGTGAACATGAGCCCTGGAT
ATIP4	ACCAGGAGGATTTCGCAGTT	TGATGACAGCGGCATTACCA

Generation of the lentiviral system

The lentiviral-based vector pLL3.7 was used to express shRNAs in PC3 cells. The oligonucleotides obtained from Invitrogen were subcloned and inserted into the lentiviral vector pLL3.7. Lentiviruses were generated in HEK293T cells by co-transfecting them with the lentiviral vector and packaging plasmids via polyethylenimine (PEI) transfection. Viral supernatants were collected 48 h after transfection, centrifuged at 75,000 *g* for 90 min, resuspended and filtered through 0.45-μm filters (Millipore, Burlington, USA). Freshly plated PC3 cells were co-cultured with the lentivirus for another 2 days. The knockdown efficiency of the *ATIP* genes was determined by western blot analysis. The oligonucleotide sequences for shRNA-targeted mRNAs used were as follows: negative control (NTC) shRNA, 5′-GCGCGCTTTGTAGGATTCG-3′; shRNA-ATIP1, 5′-GCAGGAGGGAGATTGTATT-3′; and shRNA-ATIP3, 5′-GCAGGTGTTAGATATGCAT-3′.

Western blot analysis

Total protein was extracted from cells or tissues using RIPA buffer. Protein concentration was determined following the instructions of a BCA protein assay kit (Thermo Fisher Scientific). The extracted proteins were separated by SDS-PAGE, transferred to a polyvinylidene difluoride membrane (Millipore), and blocked by 5% BSA (Sangon Biotech, Shanghai, China). The blocked membrane was incubated with the indicated primary antibodies overnight at 4°C and then with the corresponding HRP-connected second antibody for 2 h at room temperature. Finally, the membrane was detected with enhanced chemiluminesence (ECL) reagent (Vazyme Biotech Co., Ltd, Nanjing, China) according to the manufacturer's instructions.

Immunofluorescence assay

Cells were fixed in 4% formalin for 15 min at 22°C, permeabilized in 0.1% Triton X-100/PBS for 5 min, washed with PBS, and blocked in 5% normal goat serum (NGS) for 60 min. Then, cells were labeled with MitoTracker Deep Red or an appropriate primary antibody in 5% NGS/PBS and incubated overnight at 4°C. After being washed with PBS, the cells were incubated with Alexa 488- or Alexa 594-conjugated secondary antibodies (Thermo Fisher Scientific) for another 60 min at 22°C. The nuclei were stained with 4′,6-diamidino-2-phenylindole (DAPI) at a concentration of 50 μg/mL for 5 min. Finally, cells were mounted and observed under a Zeiss LSM 780 confocal microscope (Zeiss, Oberkochen, Germany).

Cell proliferation and cell cycle analysis

Cells transfected with the indicated siRNA were labeled with propidium iodide (PI) and analyzed for cell cycle distribution by flow cytometry. Alternatively, cell proliferation was quantified by direct cell counting via Trypan blue staining.

Mitochondria time-lapse video microscopy

PC3 cells (2×10^4) were seeded on glass-bottom 35-mm plates (NEST, Wuxi, China) and incubated with 100 nM MitoTracker Deep Red Dye for 20 min before fixation with 4% formalin. Then, videos were recorded on a Zeiss LSM 780 confocal microscope as previously described by Wang *et al.* [21]. Time-lapse recording was performed for 2 min, with one frame captured every 3 seconds. Under each condition, at least 5 individual cells were collected for the analysis of mitochondrial motility. The 3-dimensional (3D) videos were imported into Zeiss software to count fission and fusion events. The volume of mitochondria was analyzed for at least 8 mitochondria per area in 3D videos. The changes in mitochondrial volume were evaluated by determining the fold change over time: a fold change > 1.3 was considered a fusion event, and a fold change < 0.7 was considered a fission event. The average numbers of fission and fusion events from 8–10 areas were used for each condition's analysis.

Tumor cell motility

For 2-dimensional (2D) cell motility detection, assays were performed as previously described by Wang *et al.* [21]. PC3 cells (2×10^4) were transfected with the indicated siRNA, seeded in μ-Slide 4 Well Chambers (Ibidi, Munich, Germany), and cultured in complete medium for 24 h. The video for each area was recorded for 10 h with a time-lapse interval of 10 min by using a ×10 objective under an inverted microscope (Olympus, Tokyo, Japan). Time-lapse videos were imported into ImageJ Fiji software (NIH) for analysis by manual tracking, and at least 20 cells per condition were tracked. Subsequently, the tracking data were exported to the Chemotaxis and Migration Tool (Ibidi, v.2.0) for graphing and calculation of the mean ± SD of speed and distance of movement. The wound-closure assay was performed to evaluate directional cell migration. Wounds in PC3 cells were made with a 10-μL pipette tip, washed 3 times with PBS, and maintained in complete culture medium for 20 h of recording.

Tumor cell invasion

Tumor cell invasion experiments were performed as previously described by Wang *et al.* [21] using growth factor-reduced Matrigel-coated 8-mm polyester Transwell chambers (Corning, New York, USA). PC3 cells were seeded in a Matrigel-coated Transwell chamber (1×10^5 cells/well) in 0.1% BSA RPMI 1640 medium in triplicate, and conditional medium from NIH3T3 cells was placed in the lower chamber as a chemoattractant. After incubation for 16 h, non-invading cells were scraped off from the upper side of the membranes, and the invaded cells on the bottom side of the Transwell insert were fixed in methanol. The membranes were cut and mounted in medium containing DAPI (Vector Laboratories). Images of 5 random fields were collected at ×10 magnification for each membrane and analyzed by ImageJ software.

Animal studies

Animal studies were carried out in accordance with the Institutional Animal Care and Use Committee of the University of Electronic Science and Technology of China, and ethical approval (No. 27614) was obtained. Six- to eight-week-old male NOD-SCID mice were obtained from Beijing Vital River Laboratory Animal Technology Co., Ltd. (Beijing, China). Mice used in this study were housed under standard specific pathogen-free (SPF) conditions. To create a liver metastasis model, NOD-SCID mice (5 mice per experimental condition) were anesthetized with pentobarbital, and the abdominal cavity was exposed via laparotomy. Then, PC3 cells (1×10^6) transfected with shRNAs targeting different individual ATIP isoforms were injected into the spleen. One day after injection, the spleens were removed, and the animals were euthanized 11 days later. Thereafter, the livers were collected, fixed in formalin, and paraffin-embedded. After staining with hematoxylin and eosin (H&E), the metastatic foci were counted, and the surface area of the foci was determined using ImageJ software.

Statistical analysis

Data are expressed as the mean ± SD of multiple independent experiments or replicates of representative experiments with at least 2 or 3 independent determinations. A 2-tailed Student's *t* test was used for 2-group comparative analyses. All the statistical analyses were performed using GraphPad Prism 8 Software (La Jolla, USA). A value of $P < 0.05$ indicates a statistically significant difference.

Results

Correlation between ATIP expression and prognosis prediction in prostate cancer patients

To investigate the role and expression of ATIP in the progression of prostate cancer, we analyzed the expression of ATIP in data from the GEO database (GSE21034), which includes diverse clinicopathological parameters from 218 prostate cancer patients. As shown in Figure 1A, the *ATIP* mRNA expression level in prostate cancer tissues was markedly lower than that in normal prostate tissues. Furthermore, we tested the relationship between ATIP mRNA expression profiles and clinicopathological progression. The expression of ATIP was notably decreased in metastatic prostate cancer compared to that in primary tissue (Figure 1B). Consistently, the expression of ATIP was significantly lower in recurrent prostate cancer patients compared to that in non-recurrent patients (Figure 1C). Similarly, there was a trend toward lower ATIP expression with higher Gleason score (Figure 1D). Additionally, we used logistic regression to investigate the correlation between ATIP expression and overall survival (OS) probability. Patients were divided into

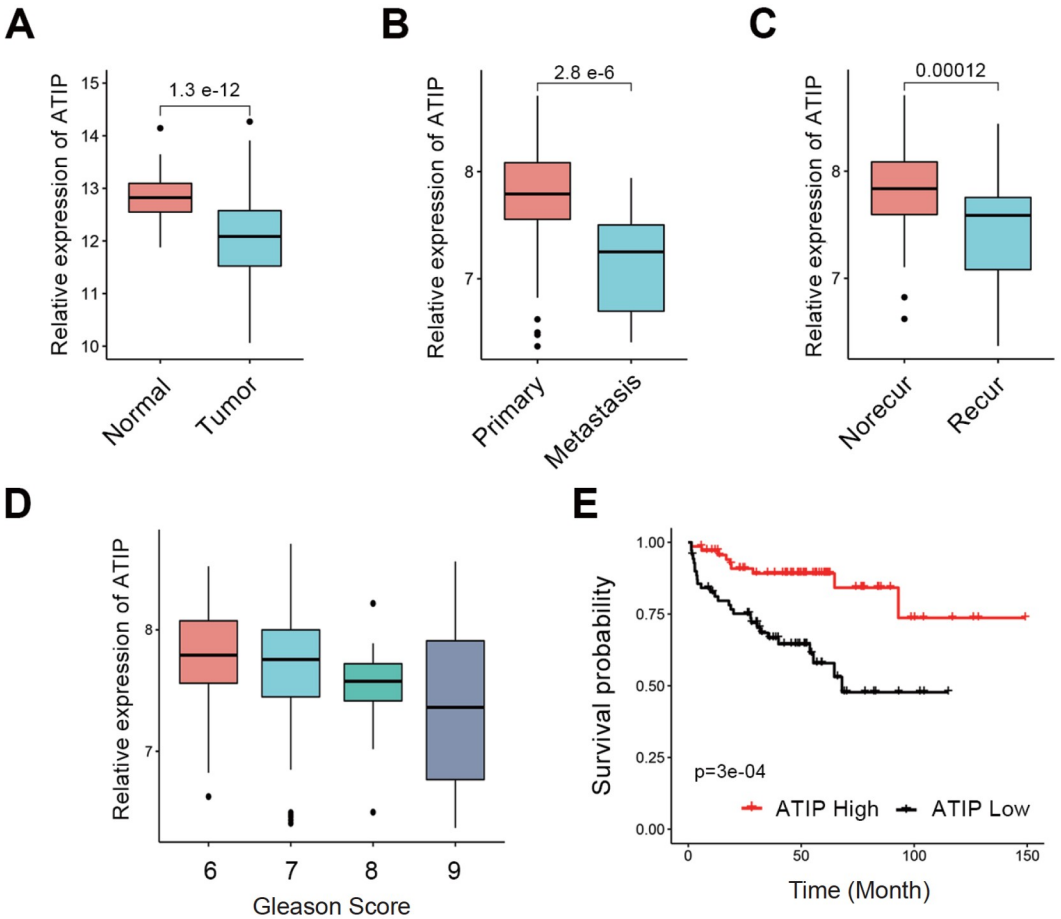

Figure 1. Expression of ATIP in prostate cancer patients Box plot of ATIP expression level between (A) normal prostate gland and prostate tumor; (B) primary and metastatic tumors; and (C) non-recurrent and recurrent patients. The *P* value was calculated by the Wilcoxon test. (D) Box plot shows the expression of ATIP in prostate cancer patients across different Gleason grades. (E) Kaplan-Meier overall survival (OS) curves for prostate cancer patients stratified by high or low ATIP expression. The *P* value was calculated by the Log-rank test.

high and low ATIP expression groups using the median expression level (50%) as the cutoff. A lower ATIP expression in prostate cancer patients was strongly associated with a poorer survival curve (Figure 1E). These results suggest that decreased ATIP expression promotes tumor progression and metastasis in prostate cancer patients. Therefore, ATIP could be a potential diagnostic and prognostic factor for prostate cancer.

ATIP1, but not ATIP3, modulates metastasis of prostate cancer cells

To understand the function of ATIP, endogenous *ATIP* in prostate cancer cells was knocked down using either individual or combined ATIP-directed siRNA sequences, and the knockdown efficiency was measured by western blot analysis (Supplementary Figure S1A). Consistent with the bioinformatics analysis, knockdown of *ATIP* by single or mixed ATIP-directed siRNA strongly promoted the migration of prostate cancer PC3 cells (Supplementary Figure S1B, C). Since both single ATIP-directed siRNA sequences strongly affected ATIP silencing and cell migration, we combined these two single siRNA sequences at a 1:1 ratio as ATIP siRNAs for subsequent experiments. In addition to migration, tumor cell proliferation is also closely linked to poor prognosis in cancer patients. However, silencing of *ATIP* did not affect cell proliferation (Supplementary Figure S1D) or cell cycle progression (Supplementary Figure S1E,F). These findings suggest that ATIP is involved in regulating metastasis rather than the proliferation of prostate cancer.

The *ATIP* gene encodes four protein isoforms in humans, each of which has unique structure and subcellular targeting sequence (Supplementary Figure S2A). Therefore, we investigated which isoform plays a critical role in prostate tumor metastasis. The expression of each isoform was examined by qPCR in the prostate cancer cell line PC3. ATIP1 and ATIP3 are the two most prominently expressed isoforms in PC3 cells (Supplementary Figure S2B). Hence, we generated ATIP1 cDNA and ATIP3 cDNA and subsequently verified their expressions by western blot analysis (Supplementary Figure S2C). Next, we reintroduced ATIP1 and ATIP3 into ATIP-knockdown PC3 cells separately, and a reversal of cell migration was observed upon reconstitution with non-siRNA-inhibitable ATIP1 cDNA but not with ATIP3 cDNA (Figure 2A,B). Accordingly, assays of cell invasion across the Matrigel-coated inserts (Figure 2C,D) and wound healing (Figure 2E,F) also confirmed that ATIP1 plays a more critical role in the invasion and migration of PC3 cells.

Tyrosine kinase focal adhesion kinase (FAK) is located at the adhesion sites of the extracellular matrix (ECM) and plays a predominant role in cellular movement. Additionally, E-cadherin and Snail are widely used biomarkers for epithelial–mesenchymal transition (EMT). PC3 cells in which *ATIP* was silenced exhibited an increase in the total protein level of Snail and the phosphorylation level of the cell motility kinase FAK at the Tyr925 site but a decrease in the protein level of E-cadherin (Figure 2G). However, reconstitution of ATIP1, but not ATIP3, attenuated the increase in the Snail protein level and the phosphorylation of FAK at the Tyr925 site in ATIP-deficient PC3 cells (Figure 2G). Taken together, these results indicate that ATIP1 is essential for the modulation of metastasis in prostate cancer PC3 cells.

ATIP1 regulates mitochondrial dynamics

Next, we explored the regulatory mechanisms of ATIP1-associated tumor cell metastasis. Since ATIP1 is a mitochondrial protein, we first examined mitochondrial morphology by MitoTracker staining. Loss of ATIP caused prominent mitochondrial fragmentation, while reintroduction of ATIP1 restored tubular mitochondrial morphology (Figure 3A). Moreover, ATIP deficiency significantly reduced the mitochondrial volume in PC3 cells, whereas reconstitution with ATIP1 cDNA largely restored the mitochondrial size to that of the control group (Figure 3B).

To investigate the role of ATIP in mediating mitochondrial dynamics, time-lapse microscopy was used for video recording. Similarly, ATIP deficiency increased mitochondrial motility (Figure 3C), resulting in a longer travel distance (Figure 3D, left) and faster mitochondrial movement (Figure 3D, right) in individual mitochondria than in control cells. Similarly, the loss of ATIP was associated with increased mitochondrial dynamics in PC3 cells (Figure 3E), which was characterized by a significantly greater frequency of fission events (Figure 3F, left) but slightly influenced fusion events (Figure 3F, right). Furthermore, these ATIP-mediated changes in mitochondrial dynamics could be effectively reversed by reintroduction of ATIP1 cDNA (Figure 3C–F).

Mechanistically, mitochondrial morphology is tightly regulated by the fission protein Drp1 and the fusion proteins MFN1 and MFN2. In accordance with the changes in mitochondrial dynamics, siRNA knockdown of *ATIP* increased the expression of MFN1 and total and Ser616-phosphorylated (the active site) Drp1, as demonstrated by western blot analysis (Figure 3G). However, the loss of ATIP failed to change the MFN2 status (Figure 3G). Collectively, these data highlight the crucial role of ATIP in triggering mitochondrial dynamics through activation of the Drp1 pathway.

Mitochondrial fission participates in ATIP-mediated tumor cell motility

Increased mitochondrial trafficking has been linked to the movement of tumor cells. Hence, a 2D cell motility assay was carried out to test this ability. Silencing of *ATIP* in PC3 cells significantly increased 2D cell motility (Supplementary Figure S3A), and the quantitative parameters of cell movement were analyzed (Supplementary Figure S3B, C). Moreover, ATIP-mediated cell motility was visibly reversed by the re-expression of ATIP1 (Supplementary Figure S3A–C).

Since Drp1 activation occurred upon *ATIP* silencing, we investigated the role of Drp1 in ATIP-mediated cell movement. *Drp1* silencing was sufficient to decrease the phosphorylation level of FAK at the Tyr925 site, which was promoted by the loss of ATIP (Figure 4A). In addition, the increase in tumor cell invasion after *ATIP* knockdown was also suppressed by the silencing of *Drp1* (Figure 4B,C). Mdivi-1, a well-known small chemical inhibitor of Drp1, consistently impeded the increase in the phosphorylation level of FAK at the Tyr925 site (Supplementary Figure S4A) and cell invasion (Supplementary Figure S4B,C), even when *ATIP* was silenced in PC3 cells. Our observations indicated that the regulation of mitochondrial fission by ATIP contributes to the invasive capability of prostate cancer cells.

Functionally, the knockdown of *Drp1* inhibited cell motility, which was triggered by the loss of ATIP (Figure 4D). Quantitative analysis also confirmed that the loss of ATIP significantly promoted the movement speed and distance of PC3 cells, whereas the silencing of *Drp1* strongly reduced the accumulated distance of cell movement (Figure 4E) and decreased the speed (Figure 4F). These

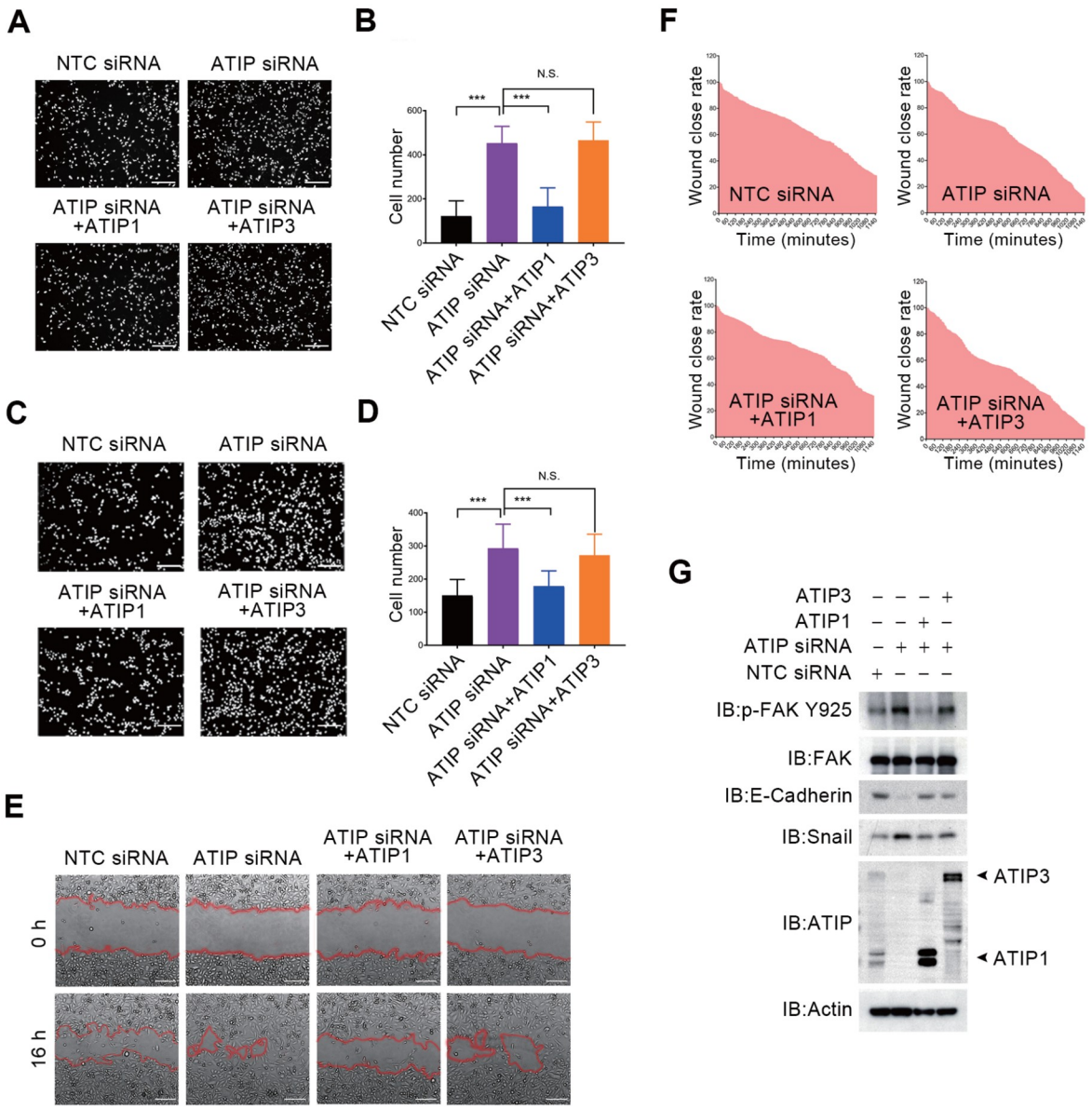

Figure 2. Role of ATIP/ATIP1 in tumor cell motility PC3 cells transfected with NTC siRNA or ATIP siRNA were reconstituted with ATIP1 or ATIP3 and then used for the subsequent analyses. (A,B) PC3 cells transfected as indicated were analyzed for migration across Transwell inserts. Representative images of DAPI-stained nuclei of migrated cells are shown (A), and the number of migrated cells was quantified for each condition (B). Scale bar: 200 μm. (C,D) PC3 cells transfected as indicated were analyzed for cell invasion across Matrigel-coated Transwell inserts. Representative images of DAPI-stained nuclei of invaded cells are shown (C), and the number of invaded cells was quantified for each condition (D). Scale bar: 200 μm. (E,F) PC3 cells transfected as indicated were analyzed for directional cell migration in a wound closure assay (E), and the area covered by cell migration was quantified at indicated time point (F). Scale bar: 200 μm. (G) PC3 cells transfected as indicated were analyzed by western blot analysis. P indicates phosphorylation. NTC siRNA, non-targeting control siRNA. ***$P < 0.0001$, N.S., not significant.

findings suggest that the loss of ATIP increases cell motility via the activation of Drp1 signaling.

ATIP1 deficiency promotes distal metastasis of tumor cells *in vivo*

To ascertain the role of ATIP1 and ATIP3 in metastasis *in vitro* and *in vivo*, we generated PC3 cells that were stably transduced with lentiviruses carrying NTC shRNA, ATIP1 shRNA or ATIP3 shRNA. The ATIP1-deficient PC3 cells exhibited greater invasion ability (Supplementary Figure S5A), and the number of invading PC3 cells in the ATIP1 shRNA-transduced group was greater than that in the NTC shRNA and ATIP3 groups (Supplementary Figure S5B).

Finally, we examined the impact of ATIP expression on systemic tumor dissemination. PC3 cells transfected with NTC shRNA, ATIP1 shRNA or ATIP3 shRNA were injected into the spleen separately. The spleen was removed 1 day after injection, and the mice were anesthetized 11 days later. By the end of the experiment, the number of metastatic foci and their areas were measured. As shown in Figure 5A, ATIP1 depletion led to a significant increase in the number and size of metastatic foci in the livers of the mice. Morphometric quantification demonstrated that *ATIP1* knockdown increased the number of metastatic foci and the overall surface area

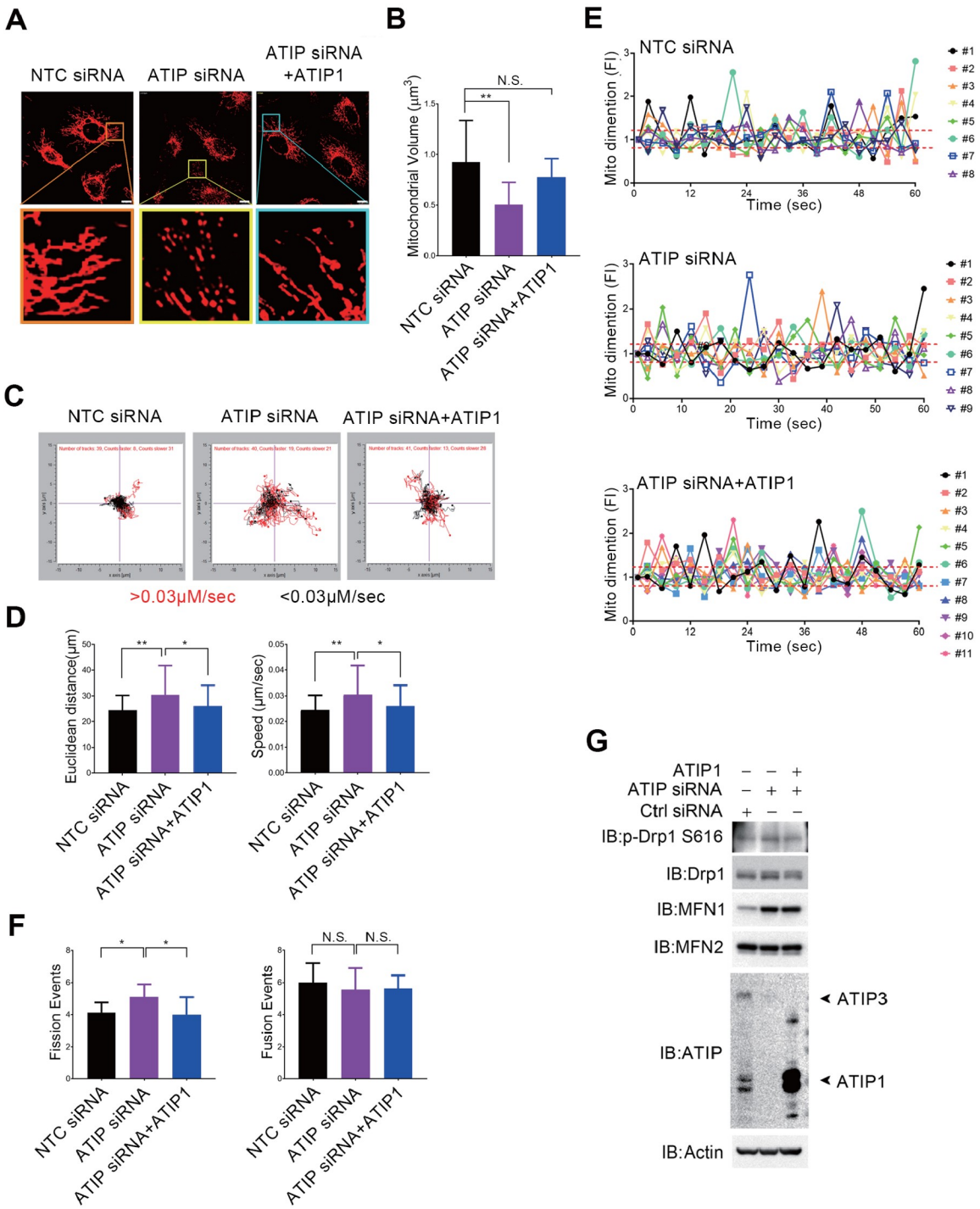

Figure 3. Role of ATIP in mitochondrial dynamics PC3 cells transfected with NTC siRNA or ATIP siRNA were reconstituted with or without ATIP1 cDNA and used for the subsequent assays. (A) PC3 cells transfected as indicated were labeled with MitoTracker Deep Red and analyzed for mitochondrial morphology by confocal laser microscopy. Representative images are shown. Insets show magnifications of the indicated areas. Scale bar: 10 μm. (B) Quantification of the mitochondrial volume for the PC3 cells transfected as indicated (n = 10–13). (C) PC3 cells transfected as indicated were analyzed for mitochondrial motility in 2D contour plots. Each tracing corresponds to the movement of an individual mitochondrion. The cutoff velocities for fast-moving (> 0.03 μm /sec, red line) or slow-moving (< 0.03 μm /sec, black line) mitochondria are indicated (n = 29–31). (D) For PC3 cells transfected as indicated, the total distance traveled by individual mitochondria (left) and the speed of mitochondrial movements (right) were quantified (n = 29–31). (E) PC3 cells transfected as indicated were analyzed for mitochondrial dynamic changes. The events were quantified continuously by time-lapse video microscopy for 60 s at a time interval of 3 s. Each tracing corresponds to an individual mitochondrion. The mitochondria with > 1.3-fold change (positive y scale) in volume was counted as organelle fusion, and that with < 0.7-fold change (negative y scale) in volume was counted as organelle fission. Representative experiment (n = 2). (F) PC3 cells were transfected as indicated, and mitochondrial fission (left) and fusion (right) events were quantified. (G) PC3 cells were transfected as indicated, and expressions of Ser616-phosphorylated Drp1, total Drp1/MFN1/MFN2 were detected by western blot analysis. NTC siRNA, non-targeting control siRNA. *P < 0.05, **P < 0.01, N.S., not significant.

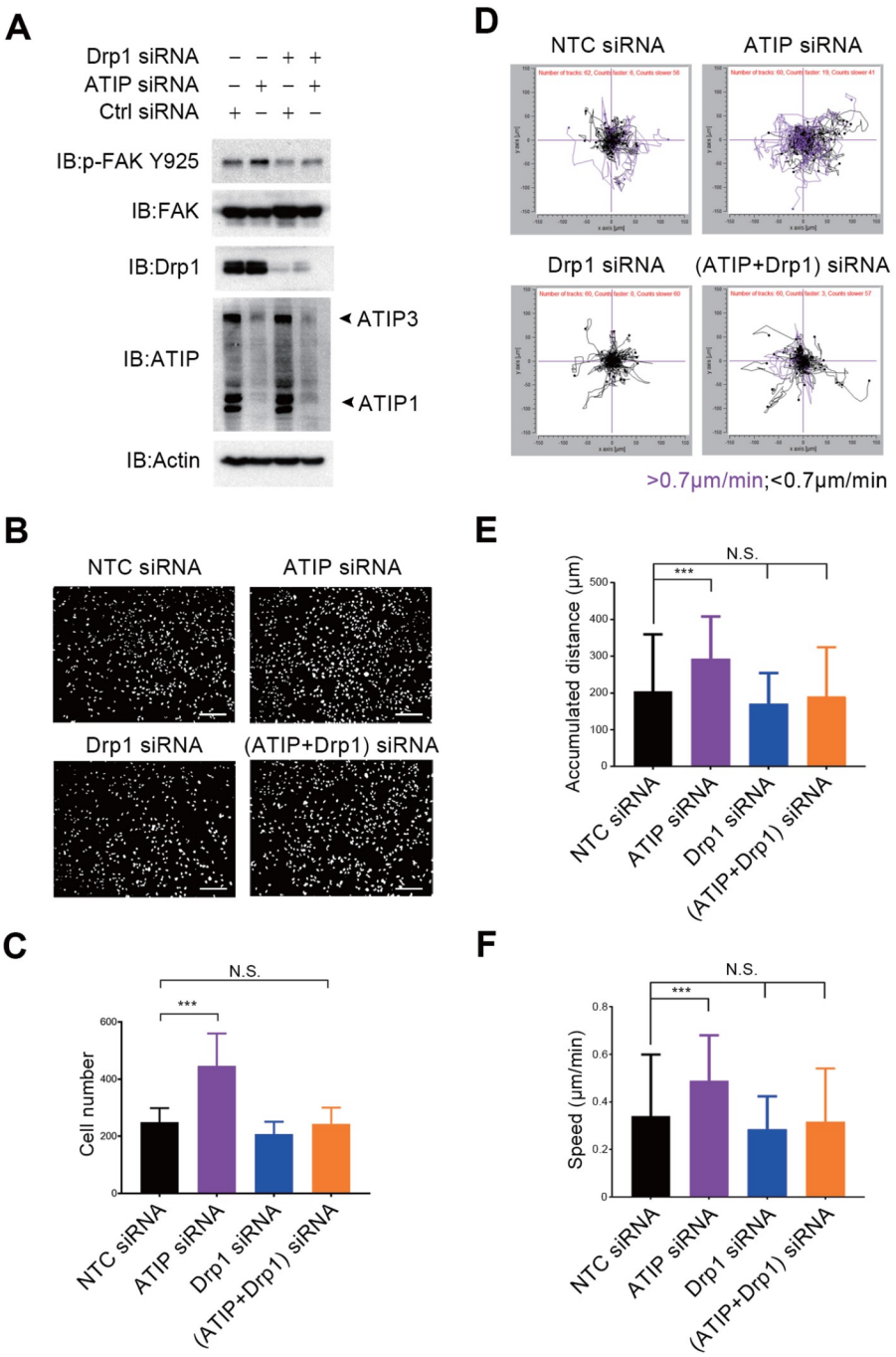

Figure 4. Regulatory role of Drp1 in ATIP-mediated tumor cell motility (A) PC3 cells transfected with NTC siRNA or ATIP siRNA were further transfected with Drp1 siRNA and analyzed by western blot analysis. (B,C) The conditions are as in (A), PC3 cells were analyzed for cell invasion across Matrigel-coated Transwell inserts. Representative images of DAPI-stained nuclei of migrated or invaded cells are shown (B), and the number of invaded cells was quantified in (C). Scale bar: 200 μm. (D–F) The conditions are the same as in (A), and PC3 cells were analyzed for cell motility in 2D contour plots. Each tracing corresponds to the movement of an individual cell. The cutoff velocities for slow-moving (< 0.7 μm/min, black line) or fast-moving (> 0.7 μm/min, purple line) cells are shown (D). The distance traveled by individual cell (E) and speed of cell movements (F) were quantified respectively ($n = 60$–62). ***$P < 0.001$, N.S., not significant.

of liver metastases (Figure 5B,C). Conversely, *ATIP3* knockdown slightly increased the number of metastatic foci (Figure 5B) but did not alter the overall area of the metastatic foci (Figure 5C).

At the molecular level, ATIP1 deficiency increased the phosphorylation of Drp1 at the S616 site but had a weak effect on the expression of Drp1 and MFN1 (Figure 5D). These findings confirm that ATIP1 deficiency indeed stimulates the distant metastasis of prostate cancer cells *in vivo*.

Discussion

In this study, we demonstrated that ATIP expression is associated with the malignancy of prostate cancer. Lower levels of ATIP

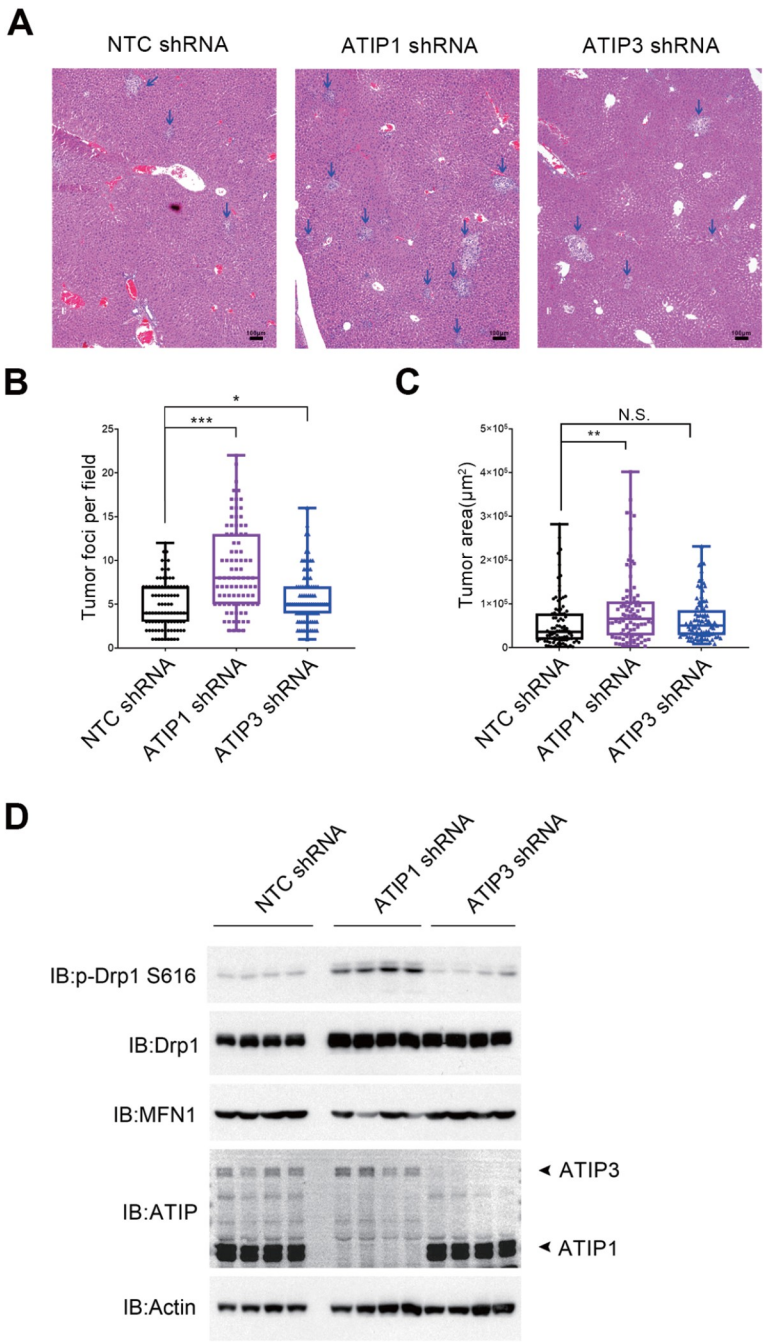

Figure 5. Physiological effect of ATIP1 on tumor cell invasion *in vivo* (A) PC3 cells stably transduced with NTC shRNA, ATIP1 shRNA or ATIP3 shRNA were separately injected into the spleens of NOD-SCID mice. The metastatic foci to the liver were identified after 14 days by hematoxylin and eosin staining and observed under a light microscope. Representative images are shown. The blue arrows indicate metastatic foci. Scale bar: 100 μm. (B,C) The conditions are the same as in A, and the number (NTC shRNA, $n = 93$; ATIP1 shRNA, $n = 89$; ATIP3 shRNA, $n = 92$) and surface area (NTC shRNA, $n = 93$; ATIP1 shRNA, $n = 89$; ATIP3 shRNA, $n = 92$) of liver metastatic foci were quantified in each animal group. (D) Effects of ATIP1 or ATIP3 on the expressions of mitochondrial dynamics-dependent signaling markers. Tumor samples were collected randomly from metastatic clones in liver tissues of each group as indicated in (A). Total Drp1, phosphorylated Drp1 S616 and total MFN1 were analyzed by western blot analysis. NTC shRNA, non-targeting control shRNA. $^{*}P < 0.05$, $^{**}P < 0.01$, $^{***}P < 0.001$, N.S., not significant.

expression were observed in patients with prostate cancer, particularly those with a higher incidence of metastasis and recurrence and elevated Gleason scores. Moreover, a reduction in ATIP expression is correlated with significantly worse survival. Functionally, the loss of endogenous ATIP enables tumor cells to exhibit increased mitochondrial dynamics, greater mitochondrial motility, and enhanced phosphorylation of oncogenic kinases; these effects are reversed by the reintroduction of ATIP1 cDNA. Consequently, the absence of ATIP leads to increased tumor cell migration and invasion, outcomes that are mitigated with ATIP1 re-expression. At the mechanistic level, the implicated pathway involves Drp1-mediated mitochondrial fission, which is essential

for the observed increase in mitochondrial dynamics and tumor cell movement both *in vivo* and *in vitro*.

ATIP was identified as a potential tumor suppressor gene. Therefore, ATIP is also called mitochondrial tumor suppressor 1 (MTUS1). The downregulation of ATIP expression has been confirmed in several types of human cancers [33,34,36]. In this study, we found that ATIP expression was significantly lower in prostate cancer tissues than in normal tissues. Moreover, patients with lower ATIP expression had greater rates of metastasis and recurrence and shorter survival. In addition, knockdown of *ATIP* in prostate cancer cells effectively increased their migration and invasion ability. These findings indicate ATIP is also a potential biomarker for prostate cancer prognosis in addition to other cancer types.

The ATIP family contains three isoforms, with ATIP1 and ATIP3 being predominantly expressed in breast cancer, colorectal cancer and prostate cancer tissues [23,32]. Clara Nahmias's group reported that the expression of the microtubule-associated protein ATIP3 is significantly reduced in highly proliferative breast carcinomas with poor clinical outcomes. Mechanistically, ATIP3 expression limits the number and size of metastases and delays the course of metastatic progression by inhibiting microtubule dynamics [27,29]. Hence, they identified ATIP3 as a prognostic biomarker for metastatic breast tumors. In addition to ATIP3, ATIP1 also plays a role in tumor progression. Overexpression of ATIP1 interferes with tumor irradiation, therapy by increasing DNA damage repair in glioblastoma [30]. Our studies revealed that ATIP1 is responsible for PC3-cell-directed migration and invasion across Matrigel-coated inserts. Loss of ATIP alters the expression levels of the cell adhesion kinases FAK, Snail and E-cadherin, and promotes cell motility, which can be reversed by re-expressing ATIP1 but not by re-expressing ATIP3. These findings suggest that ATIP1 is a potential predictive marker for prostate cancer.

Mitochondria play fundamental roles in cell survival, motility, and signal transduction. This role is controlled by mitochondrial dynamics, including morphology and ultrastructure. The shape of the mitochondria is closely associated with these dynamics, which in turn influence mitochondrial function and tumor metastasis [3,40,41]. However, there was no correlation between the mRNA expression of ATIP and the expression of mitochondrial dynamics-dependent signaling markers, as indicated by our data (not shown). The possible reason for this difference is that Drp1, the main driver of mitochondrial division, functions as a large GTPase. The mitochondrial location of Drp1 is a critical step for recruiting other fission proteins to the mitochondria to initiate fission. In addition, the phosphorylation of Drp1 at the Ser616 site ensures the enzyme's activity, which is crucial for successful fission.

Increasing evidence shows that Drp1 is a potential target for anti-tumor drug development and chemotherapy. In this study, we found that ATIP1-mediated changes in the frequency of mitochondrial fission act as key regulators of tumor migration and invasion. Blocking mitochondrial fission by transfection with Drp1 siRNA or pretreatment with Mdivi-1 retarded the increase in tumor cell motility. These results confirmed that ATIP regulates cell movement through activation of the mitochondrial fission process. Furthermore, our findings also support the idea that mitochondrial fission may be an effective anti-tumor target for prostate cancer treatment.

In summary, our study showed that ATIP is a negative regulator of prostate cancer cell movement and is a potential diagnostic biomarker for prostate cancer metastasis. An increase in ATIP1 expression retards mitochondrial fission, further decreases cell motility, and reduces the likelihood of distant metastasis.

Supplementary Data

Supplementary data is available at *Acta Biochimica et Biophysica Sinica* online.

Funding

This work was supported by the grants from the Department of Science and Technology of Sichuan Province (Nos. 2021ZYD0092 and 2022NSFSC0721), and the Fundamental Research Funds for the Central Universities (Nos. ZYGX2021J024 and Y030222059002005).

Conflict of Interest

The authors declare that they have no conflict of interest.

References

1. Hanahan D, Weinberg RA. Hallmarks of cancer: the next generation. *Cell* 2011, 144: 646–674
2. Martínez-Reyes I, Chandel NS. Cancer metabolism: looking forward. *Nat Rev Cancer* 2021, 21: 669–680
3. Quintana-Cabrera R, Scorrano L. Determinants and outcomes of mitochondrial dynamics. *Mol Cell* 2023, 83: 857–876
4. Dhingra R, Kirshenbaum LA. Regulation of mitochondrial dynamics and cell fate. *Circ J* 2014, 78: 803–810
5. Kasahara A, Scorrano L. Mitochondria: from cell death executioners to regulators of cell differentiation. *Trends Cell Biol* 2014, 24: 761–770
6. Giacomello M, Pyakurel A, Glytsou C, Scorrano L. The cell biology of mitochondrial membrane dynamics. *Nat Rev Mol Cell Biol* 2020, 21: 204–224
7. Eura Y. Two mitofusin proteins, mammalian homologues of FZO, with distinct functions are both required for mitochondrial fusion. *J Biochem* 2003, 134: 333–344
8. Misaka T, Miyashita T, Kubo Y. Primary structure of a dynamin-related mouse mitochondrial GTPase and its distribution in brain, subcellular localization, and effect on mitochondrial morphology. *J Biol Chem* 2002, 277: 15834–15842
9. Smirnova E, Griparic L, Shurland DL, van der Bliek AM. Dynamin-related protein Drp1 is required for mitochondrial division in mammalian cells. *Mol Biol Cell* 2001, 12: 2245–2256
10. James DI, Parone PA, Mattenberger Y, Martinou JC. HFis1, a novel component of the mammalian mitochondrial fission machinery. *J Biol Chem* 2003, 278: 36373–36379
11. Gandre-Babbe S, van der Bliek AM. The novel tail-anchored membrane protein Mff controls mitochondrial and peroxisomal fission in mammalian cells. *Mol Biol Cell* 2008, 19: 2402–2412
12. Zong WX, Rabinowitz JD, White E. Mitochondria and cancer. *Mol Cell* 2016, 61: 667–676
13. Trotta AP, Chipuk JE. Mitochondrial dynamics as regulators of cancer biology. *Cell Mol Life Sci* 2017, 74: 1999–2017
14. Missiroli S, Perrone M, Genovese I, Pinton P, Giorgi C. Cancer metabolism and mitochondria: finding novel mechanisms to fight tumours. *eBioMedicine* 2020, 59: 102943
15. Qiu X, Li Y, Zhang Z. Crosstalk between oxidative phosphorylation and immune escape in cancer: a new concept of therapeutic targets selection. *Cell Oncol* 2023, 46: 847–865
16. Legaki AI, Moustakas II, Sikorska M, Papadopoulos G, Velliou RI,

Chatzigeorgiou A. Hepatocyte mitochondrial dynamics and bioenergetics in obesity-related non-alcoholic fatty liver disease. *Curr Obes Rep* 2022, 11: 126–143

17. Zhao J, Zhang J, Yu M, Xie Y, Huang Y, Wolff DW, Abel PW, *et al.* Mitochondrial dynamics regulates migration and invasion of breast cancer cells. *Oncogene* 2013, 32: 4814–4824
18. Kashatus JA, Nascimento A, Myers LJ, Sher A, Byrne FL, Hoehn KL, Counter CM, *et al.* Erk2 Phosphorylation of Drp1 promotes mitochondrial fission and MAPK-driven tumor growth. *Mol Cell* 2015, 57: 537–551
19. Serasinghe MN, Wieder SY, Renault TT, Elkholi R, Asciolla JJ, Yao JL, Jabado O, *et al.* Mitochondrial division is requisite to RAS-induced transformation and targeted by oncogenic MAPK pathway inhibitors. *Mol Cell* 2015, 57: 521–536
20. Hagenbuchner J, Kuznetsov AV, Obexer P, Ausserlechner MJ. BIRC5/Survivin enhances aerobic glycolysis and drug resistance by altered regulation of the mitochondrial fusion/fission machinery. *Oncogene* 2013, 32: 4748–4757
21. Wang Y, Agarwal E, Bertolini I, Ghosh JC, Seo JH, Altieri DC. IDH2 reprograms mitochondrial dynamics in cancer through a HIF-1α-regulated pseudohypoxic state. *FASEB J* 2019, 33: 13398–13411
22. Seo JH, Agarwal E, Bryant KG, Caino MC, Kim ET, Kossenkov AV, Tang HY, *et al.* Syntaphilin ubiquitination regulates mitochondrial dynamics and tumor cell movements. *Cancer Res* 2018, 78: 4215–4228
23. Di Benedetto M, Bièche I, Deshayes F, Vacher S, Nouet S, Collura V, Seitz I, *et al.* Structural organization and expression of human MTUS1, a candidate 8p22 tumor suppressor gene encoding a family of angiotensin II AT2 receptor-interacting proteins, ATIP. *Gene* 2006, 380: 127–136
24. Haykal MM, Rodrigues-Ferreira S, Nahmias C. Microtubule-associated protein ATIP3, an emerging target for personalized medicine in breast cancer. *Cells* 2021, 10: 1080
25. Rodrigues-Ferreira S, Di Tommaso A, Dimitrov A, Cazaubon S, Gruel N, Colasson H, Nicolas A, *et al.* 8p22 MTUS1 gene product ATIP3 is a novel anti-mitotic protein underexpressed in invasive breast carcinoma of poor prognosis. *PLoS One* 2009, 4: e7239
26. Velot L, Molina A, Rodrigues-Ferreira S, Nehlig A, Bouchet BP, Morel M, Leconte L, *et al.* Negative regulation of EB1 turnover at microtubule plus ends by interaction with microtubule-associated protein ATIP3. *Oncotarget* 2015, 6: 43557–43570
27. Molina A, Velot L, Ghouinem L, Abdelkarim M, Bouchet BP, Luissint AC, Bouhlel I, *et al.* ATIP3, a novel prognostic marker of breast cancer patient survival, limits cancer cell migration and slows metastatic progression by regulating microtubule dynamics. *Cancer Res* 2013, 73: 2905–2915
28. Nehlig A, Seiler C, Steblyanko Y, Dingli F, Arras G, Loew D, Welburn J, *et al.* Reciprocal regulation of Aurora kinase A and ATIP3 in the control of metaphase spindle length. *Cell Mol Life Sci* 2021, 78: 1765–1779
29. Rodrigues-Ferreira S, Nehlig A, Kacem M, Nahmias C. ATIP3 deficiency facilitates intracellular accumulation of paclitaxel to reduce cancer cell migration and lymph node metastasis in breast cancer patients. *Sci Rep* 2020, 10: 13217
30. Ranjan N, Pandey V, Panigrahi MK, Klumpp L, Naumann U, Babu PP. The tumor suppressor MTUS1/ATIP1 modulates tumor promotion in glioma: association with epigenetics and DNA repair. *Cancers* 2021, 13: 1245
31. Chen Z, Liu X, Wang C, Jin Y, Wang Y, Wang A, Zhou X. p53 regulates the expression of human angiotensin II AT2 receptor interacting protein (ATIP1) gene. *Oncol Lett* 2011, 2: 919–922
32. Jee S, Kim H, Bang S, Kim Y, Park HY, Paik SS, Sim J, *et al.* Low-Level Expression of MTUS1 is associated with poor survival in patients with lung adenocarcinoma. *Diagnostics* 2021, 11: 1250
33. Cheng LY, Huang M, Zhong HG, Ru HM, Mo SS, Wei CY, Su ZJ, *et al.* MTUS1 is a promising diagnostic and prognostic biomarker for colorectal cancer. *World J Surg Onc* 2022, 20: 257
34. Xiao J, Chen JX, Zhu YP, Zhou LY, Shu QA, Chen LW. Reduced expression of MTUS1 mRNA is correlated with poor prognosis in bladder cancer. *Oncol Lett* 2012, 4: 113–118
35. Zhao T, Ding X, Chang B, Zhou X, Wang A. MTUS1/ATIP3a down-regulation is associated with enhanced migration, invasion and poor prognosis in salivary adenoid cystic carcinoma. *BMC Cancer* 2015, 15: 203
36. Sim J, Wi YC, Park HY, Park SY, Yoon YE, Bang S, Kim Y, *et al.* Clinicopathological significance of MTUS1 expression in patients with renal cell carcinoma. *Anticancer Res* 2020, 40: 2961–2967
37. Litwin MS, Tan HJ. The diagnosis and treatment of prostate cancer. *JAMA* 2017, 317: 2532–2542
38. Louis SNS, Chow L, Rezmann L, Krezel MA, Catt KJ, Tikellis C, Frauman AG, *et al.* Expression and function of ATIP/MTUS1 in human prostate cancer cell lines. *Prostate* 2010, 70: 1563–1574
39. Louis SNS, Chow LTC, Varghayee N, Rezmann LA, Frauman AG, Louis WJ. The expression of MTUS1/ATIP and its major isoforms, ATIP1 and ATIP3, in human prostate cancer. *Cancers* 2011, 3: 3824–3837
40. Boulton DP, Caino MC. Mitochondrial fission and fusion in tumor progression to metastasis. *Front Cell Dev Biol* 2022, 10: 849962
41. Xing J, Qi L, Liu X, Shi G, Sun X, Yang Y. Roles of mitochondrial fusion and fission in breast cancer progression: a systematic review. *World J Surg Onc* 2022, 20: 331